BIOCHEMISTRY
including biophysical chemistry & molecular biology

Article

pubs.acs.org/biochemistry

Electron-Transfer Pathways in the Heme and Quinone-Binding Domain of Complex II (Succinate Dehydrogenase)

Robert F. Anderson,*[,†] Sujata S. Shinde,[†] Russ Hille,[‡] Richard A. Rothery,[§] Joel H. Weiner,[§] Sany Rajagukguk,[∥] Elena Maklashina,[∥,⊥] and Gary Cecchini*[,∥,⊥]

[†]Auckland Cancer Society Research Centre, Faculty of Medical and Health Sciences, The University of Auckland, Auckland 1142, New Zealand

[‡]Department of Biochemistry, University of California, Riverside, California 92521, United States

[§]Membrane Protein Research Group, Department of Biochemistry, University of Alberta, Alberta T6G 2H7, Canada

[∥]Molecular Biology Division, San Francisco VA Medical Center, San Francisco, California 94121, United States

[⊥]Department of Biochemistry & Biophysics, University of California, San Francisco, California 94158, United States

Supporting Information

ABSTRACT: Single electron transfers have been examined in complex II (succinate:ubiquinone oxidoreductase) by the method of pulse radiolysis. Electrons are introduced into the enzyme initially at the [3Fe−4S] and ubiquinone sites followed by intramolecular equilibration with the *b* heme of the enzyme. To define thermodynamic and other controlling parameters for the pathways of electron transfer in complex II, site-directed variants were constructed and analyzed. Variants at SdhB-His207 and SdhB-Ile209 exhibit significantly perturbed electron transfer between the [3Fe−4S] cluster and ubiquinone. Analysis of the data using Marcus theory shows that the electronic coupling constants for wild-type and variant enzyme are all small, indicating that electron transfer occurs by diabatic tunneling. The presence of the ubiquinone is necessary for efficient electron transfer to the heme, which only slowly equilibrates with the [3Fe−4S] cluster in the absence of the quinone.

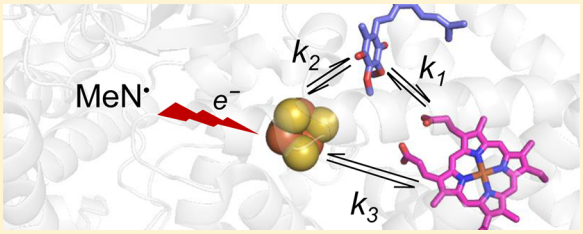

Succinate-quinone oxidoreductase (SQR), or succinate dehydrogenase, is complex II of the mitochondrial respiratory chain and is also found in many aerobic and facultative microorganisms. The enzyme, as part of the tricarboxylic acid (TCA) cycle, oxidizes succinate to fumarate, and the electrons produced by this reaction are transferred through a series of redox-active centers to the membrane quinone pool, thus providing reducing equivalents to the respiratory chain that are used for oxidative phosphorylation in the cell.[1,2] Thus, complex II plays an important role in energy-generation pathways, and it is known that homozygous knockout of the complex is embryonic lethal in mammals.[3] The SQR enzyme complex is a member of a large family of related enzymes, which, in addition to succinate dehydrogenase, include a number of related enzymes involved in anaerobic or microaerophilic metabolism in facultative bacteria or lower eukaryotes, termed quinol-fumarate reductase (QFR).[1,2,4]

In higher eukaryotes and *Escherichia coli*, complex II is a membrane-integral heterotetramer oriented toward the matrix in mitochondria and the cytoplasm in bacterial inner membranes. The enzyme is composed of hydrophilic FAD- and iron−sulfur-containing subunits bound to a two-subunit hydrophobic membrane anchor. The SdhA subunit (~66 kDa) contains a covalently bound FAD and the dicarboxylate binding site. The SdhB subunit (~27 kDa) contains three distinct iron−sulfur clusters, $[2Fe{-}2S]^{2+,1+}$, $[4Fe{-}4S]^{2+,1+}$, and $[3Fe{-}4S]^{1+,0}$, arranged to facilitate electron transfer from the flavin to the ubiquinone-binding site.[5−7] The membrane-integral SdhC (~15 kDa) and SdhD (~13 kDa) subunits, each possessing three transmembrane helices, harbor a low-spin heme *b* coordinated by a histidyl residue from each subunit as well as the quinone-binding site (also composed of amino acid residues from the SdhB subunit).[5,7−9] It is known that the heme is not essential for catalysis in complex II,[10,11] although it clearly plays a role in stabilizing the enzyme complex.[10,12] Because of its relatively high reduction potential (E_m = +36 mV),[9] the heme *b* of the *E. coli* enzyme is reducible by succinate,[13] whereas that of bovine complex II (E_m = −185 mV) is not.[14,15]

The *E. coli* SQR has proven to be a useful model for studying electron transfer and the role of quinones[16] in the complex II family of enzymes. This has been facilitated by the known X-ray crystal structure of the complex and disposition of the redox-active centers within it,[5,9] the ease of genetic manipulation, and the ability to produce significant amounts of wild-type and mutant proteins.[17,18] The redox-active centers of complex II are arranged in an approximately linear array from the FAD of

Received: December 5, 2013
Revised: February 19, 2014
Published: February 21, 2014

SdhA to the [2Fe−2S], [4Fe−4S], and [3Fe−4S] clusters in SdhB. The apparent electron-transfer pathway(s) then bifurcate, with the quinone and heme sites being approximately 7 and 8.3 Å (edge-to-edge, respectively) from the [3Fe−4S] cluster and 7.6 Å from one another (again, edge-to-edge). Overall, the intersite distances are well within the 14 Å distance thought to represent the limit for effective electron transfer in proteins.[19] Given its fundamental importance as well as the accumulating evidence regarding the enzyme's role in formation of reactive oxygen species, which may contribute to disease,[20−22] it is important to understand electron transfer in complex II. Previously, we have used the method of pulse radiolysis to investigate the kinetics and thermodynamics of electron transfer in wild-type complex II[23] as well as in other redox-active enzymes such as xanthine oxidase and trimethylamine dehydrogenase.[24,25] With this method, radiolytically generated reducing equivalents are rapidly introduced into the enzyme under well-defined conditions and subsequent intramolecular electron equilibration is followed spectrophotometrically.

These previous studies have suggested that in *E. coli* SQR the heme *b* is in oxidation−reduction equilibrium with the iron−sulfur clusters of the enzyme.[23] Conventional kinetics in conjunction with EPR spectroscopy have also suggested that the presence of quinone facilitates reduction of the heme in *E. coli* SQR.[16] To date, however, it has not been possible to obtain a full description of the thermodynamic parameters driving electron transfer or to establish essential structural features of the electron-transfer pathways from the iron−sulfur cluster relay to the ubiquinone (UQ) or *b* heme. Here, we have used pulse radiolysis in conjunction with site-directed mutagenesis and a potent quinone site inhibitor[26] to probe the electron-transfer pathways in *E. coli* SQR further. These studies enable us to refine our previous kinetic model[23] and to define thermodynamic parameters. We demonstrate that effective electron transfer between the [3Fe−4S] cluster and ubiquinone is essential for rapid reduction of the heme; we also are able to define the kinetic and thermodynamic parameters fully for electron transfer in the context of Marcus theory and to establish that electron transfer occurs via diabatic electron tunneling.

EXPERIMENTAL PROCEDURES

Strains, Plasmids, Growth Conditions, and Site-Directed Mutagenesis. *E. coli* strain DW35 (Δ*frdABCD, sdhC:kan)* is completely deficient in chromosomally encoded SQR protein[27] and was used as the host for expression of plasmid-encoded mutant or wild-type SQR. DW35 transformed with plasmid pFAS[17] ($sdhC^{+}D^{+}A^{+}B^{+}$) was used for expression of wild-type SQR following growth on LB medium under microaerophilic conditions, as described previously.[17] Mutations were constructed using the QuikChange II (Agilent Technologies) site-directed mutagenesis kit as previously described[17] using appropriate forward and reverse mutagenic primers in the PCR reaction.

Protein Expression and Purification. Wild-type and variant SQR proteins were expressed and purified following minor modifications of published procedures.[12,18] Briefly, membranes were resuspended in 20 mM potassium phosphate (pH 7.5), 0.1 mM EDTA, and complete protease inhibitor tablets (Roche). Triton X-100 was then added from a stock solution to a final concentration of 2% (w/v), giving a final ratio of approximately 5 mg of protein to 1 mL of detergent added. Triton X-100 is used to remove the endogenous quinone from the enzyme, whereas the detergent usually used ($C_{12}E_9$, Anatrace, Maumee, OH) retains the endogenous quinone. The homogenate was stirred briefly (∼15 min) at 4 °C and then sedimented by centrifugation at 100 000*g* for 1 h. The supernatant was then filtered through a 0.2 μm nylon filter and kept on ice until chromatography. The dark reddish-brown supernatant was then loaded onto a DEAE-Sepharose FF column equilibrated with 50 mM potassium phosphate (pH 7.5), 0.1 mM EDTA, and 0.05% (v/v) $C_{12}E_9$ (polyoxyethylene (9) dodecyl ether) was used to exchange the Triton X-100. The DEAE-Sepharose column is washed with two column volumes of the buffer and then with three column volumes of the same buffer containing 0.1 M NaCl, and the SQR containing fractions are then eluted with a gradient from 0.1 to 0.5 M NaCl in the same buffer. The dark reddish-brown-containing SQR fractions are then combined and concentrated using Amicon Centricon-30 filtration units. The enzyme is then stored at approximately 50 mg/mL of protein in liquid N_2 until use.

Pulse Radiolysis. The Dynaray 4 MV linear accelerator facility at the University of Auckland, New Zealand and radical detection system was used for the pulse radiolysis studies as previously described.[23] The experimental conditions used (N_2O-saturated solutions containing 0.1 M sodium formate and 2.5 mM *N*-methylnicotinamide, NMN) produce radiolytic products of water that are quantitatively converted (0.68 μM/Gy) to the strongly reducing $MeN^{\bullet}$ radical ($E_m = -1.01$ V),[28] which represents the proximal reductant of the enzyme. Typically, 3 Gy radiation doses producing 2 μM $MeN^{\bullet}$ radicals in 200 ns were used to initiate the reactions. Spectral data is obtained as the change in extinction coefficient relative to the prepulsed fully oxidized enzyme, assuming the $MeN^{\bullet}$ radical is fully scavenged by the enzyme. Previous studies have shown that the $MeN^{\bullet}$ radicals react with SQR, xanthine oxidase, and trimethylamine dehydrogenase with second-order rate constants in excess of 10^8 M^{-1} s^{-1},[23−25] allowing one to use spectrophotometric methods to follow subsequent slower (but in excess of 10^4 s^{-1}) intramolecular electron-transfer reactions. Thermodynamic parameters were determined from the temperature dependence of accessible rate constants over the range 10−35 °C using a temperature-controlled cell.

Enzyme Activity. Steady-state succinate oxidation with the artificial electron acceptor phenazine ethosulfate (PES) and the ubiquinone analogue UQ_1 was coupled to the reduction of 2,6-dichlorophenol-indophenol (DCIP) as previously described.[9,17,29] As a control for the experimental conditions used during pulse radiolysis, it was found that there was no affect of addition of 0.1 M formate or 2.5 mM NMN on the steady-state kinetics of SQR (data not shown).

Potentiometric Titrations and EPR Spectroscopy. Potentiometric titrations for the [3Fe−4S] cluster were carried out on membrane preparation enriched with wild-type and mutant SQR enzymes at 25 °C as previously described.[30,31] Titrations were carried out at pH 7.0 in a buffer containing 0.1 M MOPS, 5 mM EDTA, and 1 mM malonate. EPR spectra were acquired with a Brüker Elexsys E500 spectrometer equipped with a Brüker SHQE cavity and an Oxford Instruments ESR900 flowing helium cryostat. The EPR spectra from the $[3Fe-4S]^{1+,0}$ center were recorded at 12 K (20 mW microwave power and 100 kHz modulation frequency). The [3Fe−4S] spectra were recorded at modulations amplitudes of

10 G_{pp}. Five scans were accumulated for each sample. Reported E_m values are accurate within ca. ±10 mV.

RESULTS

Pulse Radiolysis of Wild-Type and Variant SQR. The spectral changes observed upon reduction of the several chromophores of wild-type *E. coli* SQR have been defined previously in titrations with sodium dithionite,[23] making it possible to ascribe absorbance changes at different wavelengths to reduction of the FAD, iron−sulfur, and heme centers of the enzyme. Bleaching of absorbance in the 440−510 nm region is primarily due to reduction of the flavin and iron−sulfur clusters of the enzyme[23] (as noted in Figure 1 of ref 23), whereas absorbance increases in the 420−435 nm region (and also 558 nm) are principally due to reduction of the *b* heme.[23] Previously, using wild-type SQR and pulse radiolysis, three kinetic phases were observed for intramolecular electron transfers (i.e., independent of enzyme concentration) following reduction of the enzyme by the MeN• radical at a biomolecular rate constant (k_0) of 7×10^8 M^{-1} s^{-1} (the three kinetic phases are shown in Figure 4 of ref 23, whereas a partial kinetic scheme is shown in Figure 9 of the same reference). The loss in the minor absorbance of the MeN• radical at 450 nm for low concentrations of the enzyme lead to a small amount of bleaching of the enzyme at this wavelength,[23] which together with other observed spectral changes on the same time scale identify this as heme reduction. At concentrations above ~30 μM enzyme, this fast bleaching of the enzyme occurred with no observable increase in rate constant. This plateau in rate constant we now designate to be k_1 and can be ascribed to an electron-transfer pathway between UQ and heme ($k_1 \sim 24\,000$ s^{-1}), as shown in Figure 1, rather than arising from some

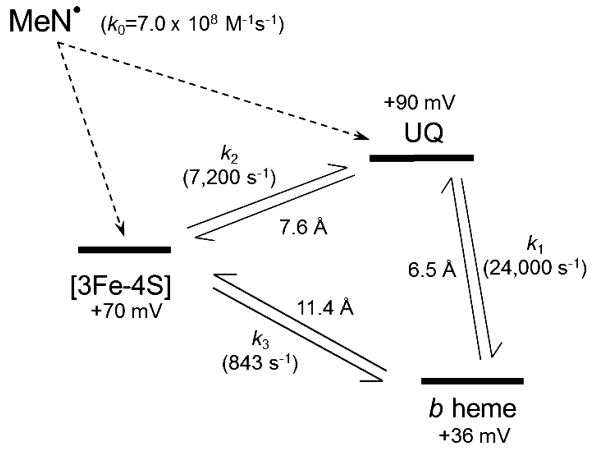

Figure 1. One-electron reduction and subsequent rates of equilibration of the reducing equivalent over the distances between redox-active centers of wild-type SQR.

association between the *N*-methylnicotinamide and SQR. The reinterpretation of this data is consistent with the short distance between UQ and heme and accounts for the rapid appearance of reduced heme through electron transfer from ubisemiquinone, which is produced in a minor amount upon reaction of the MeN• radical with the enzyme. The previous rate-determining step for the large reduction of the heme from the reduced [3Fe−4S] (i.e., electron transfer between the [3Fe−4S] and UQ) observed at 430 nm (formerly termed k_1)[23] occurs at a slower rate of ~7200 s^{-1} and is now designated as k_2 in Figure 1. The slowest of the three intramolecular electron-transfer processes (i.e., between the [3Fe−4S] and the heme) representing k_3 (~843 s^{-1}, Figure 1) is the third kinetic pathway and had previously be termed k_2.[23] The modified assignment of intramolecular kinetic pathways observed for the wild-type protein is the in order of the relative distances of the three redox centers from one another (Figure 1).

We have extended these studies by examining variants of SQR designed to interfere with potential electron-transfer pathways from the [3Fe−4S] center to UQ and to the *b* heme. Optimal electron-transfer pathways between the [3Fe−4S], UQ, and heme have been analyzed using the program HARLEM (http://harlem.chem.cmu.edu), with two different X-ray structures of wild-type SQR in complex with either ubiquinone (PDB code 1NEK at 2.6 Å resolution[5]) or the inhibitor carboxin (PDB code 2WDQ, at 2.4 Å resolution[32]). The HARLEM analysis indicates that three amino acids, SdhB-Pro160, SdhB-His207, and SdhB-Ile209, are part of the electron-transfer pathway from the [3Fe−4S] center to the UQ and heme moieties of SQR (Figure 2). In the structure of the ubiquinone complex (1NEK), the primary electron-transfer path between the [3Fe−4S] center and UQ involves two through-space jumps via Ile-209 of SdhB (path 2, Figure 2). When Ile-B209 is mutated *in silico* to Ala, a secondary electron-transfer pathway is identified involving covalent bonds of Cys-159 and Pro-160 of SdhB and a through-space jump to UQ

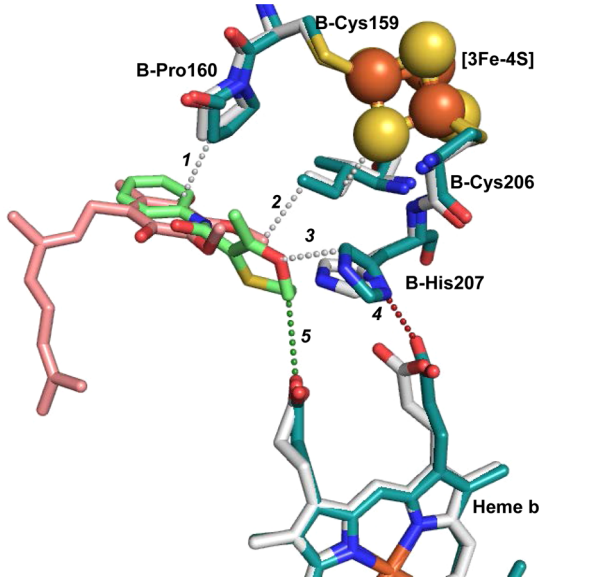

Figure 2. Proposed electron-transfer pathways between the [3Fe−4S] cluster to UQ and heme *b* of SQR. The [3Fe−4S] center is shown in red and gold spheres, UQ is shown in pink, and the UQ-site inhibitor carboxin is shown in light green. Protein Data Bank code 1NEK was used to derive the wild-type structure with UQ present, and PDB code 2WDQ was used to derive the structure with carboxin. At the bottom of the figure is shown the heme *b* in gray for the wild-type structure and in green-blue for the structure with carboxin. The HARLEM program was used to derive potential electron-transfer pathways between the [3Fe−4S] center and the UQ-binding site, with three potential pathways show by the gray dotted lines (1−3). Pathways 1 and 2 were determined with UQ present, and pathway 3 was determined using the UQ-site inhibitor carboxin (path 3). The dotted red lines show path 4 between the [3Fe−4S] and heme, which is the same for both structures. The green dotted spheres show path 5 between the heme *b* and the UQ-site when carboxin is present.

dx.doi.org/10.1021/bi401630m | *Biochemistry* 2014, 53, 1637−1646

Table 1. Comparison of Succinate-Oxidase Reactions Catalyzed by SQR Enzymes[a]

	succinate-PES	succinate-UQ1		E_m [3Fe−4S] cluster
	TN (s^{-1})	K_m, μM	TN (s^{-1})	
wild-type SQR	98	3.5	101	+70 mV[b]
SdhB-Ile209Ala	93	5.7	21	+125 mV
SdhB-Ile209Lys	90	nd	<1	+150 mV
SdhB-His207Thr	92	8.8	89	+2 mV[b]
SdhB-Pro160Gly	79	5.2	32	nd
SdhB-Pro160Gly/Ile209Ala	82	5.8	12	nd

[a]Isolated SQR enzymes were activated with 3 mM malonate (pH 7, 30 °C for 20 min), and the succinate activities were determined with PES (phenazine ethosulfate) and UQ_1 in 50 mM Bis-Tris-Propane, pH 8, as previously described.[29,31]. TN, turnover number based on heme *b* content of enzyme preparations. nd, not determined. [b]Data taken from Tran et al.[10] and Ruprecht et al.,[9] respectively.

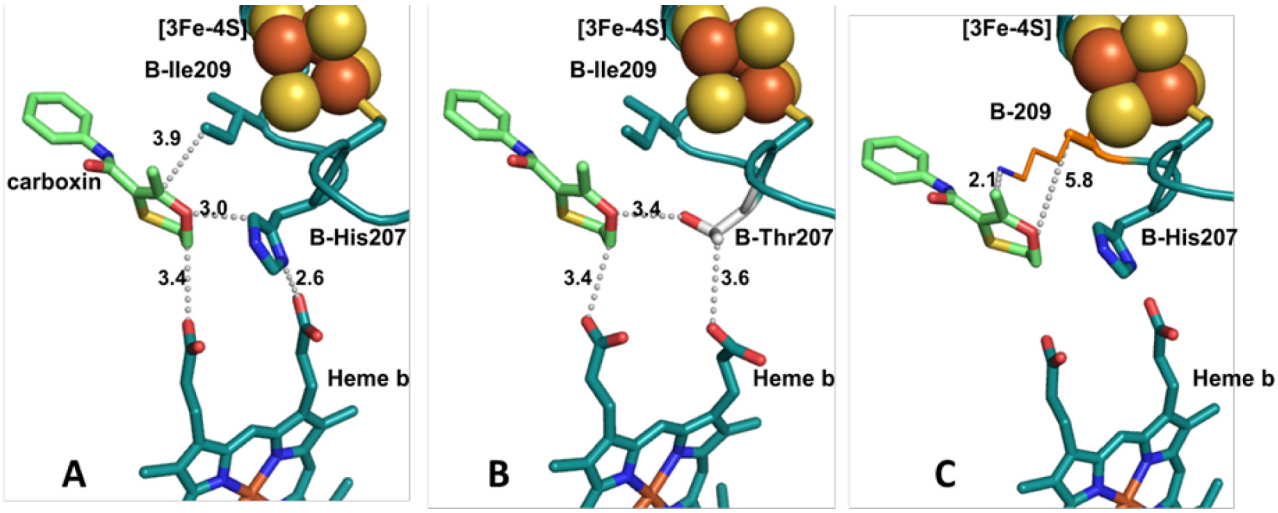

Figure 3. Electron-transfer distances in SQR. (A) Wild-type SQR structure with carboxin (PDB code 2WDQ). (B) SdhB-His207Thr variant enzyme structure (PDB code 2WP9). (C) *In silico* derived structure of SdhB-Ile209 variant enzymes. The Ile209Ala variant is shown as the thick orange line, and the Ile209Lys variant enzyme is shown as the thin gold line with the N-ε-amino group of the Lys shown in blue. The gray dotted spheres show the gaps between nearest atoms between the redox-active centers, and nearest distances are indicated in angstroms. The *in silico* structure indicated that the SdhB-209Lys substitution would likely clash with UQ or carboxin at the UQ-binding site.

(path 1, Figure 2). The analysis of the carboxin-bound structure (2WDQ) suggests an alternate path through backbone covalent bonds of Cys-206 and His-207 of SdhB, then a through-space jump from the CD2 atom of the imidazole ring of His-207, and then on to carboxin (path 3, Figure 2). The heme *b* D-ring propionate is approximately 8.2 and 8.4 Å from the [3Fe−4S] cluster in the two SQR structures, with the same electron-transfer pathway determined for the electron transfer between the heme and Fe−S center (path 4, Figure 2). This pathway also involves Cys-206 and His-207 with through-space jumps between atom ND1 of the imidazole and the O2D oxygen atom of the D-ring heme propionate. Lastly, the calculated electron-transfer pathway between the heme *b* and UQ depends on the position of the quinoid ring in the UQ-binding pocket. In the 2WDQ structure, the carboxin, which we suggest represents the position of UQ_1 is approximately 3 Å from His-207 and thus would allow direct electron transfer between two redox-active groups (path 5, Figure 2).

An initial steady-state survey of several variants was conducted to choose those most appropriate for pulse radiolysis experiments. Steady-state kinetic assays of wild-type SQR and variants are shown in Table 1. All enzyme forms retain essentially full succinate-oxidase activity in the succinate-PES assay, indicating that the amino acid substitutions have not perturbed the ability of the enzyme to oxidize succinate and that the enzyme is fully assembled. It has previously been shown that the SdhB-His207Thr variant retains near wild-type activity in its ability to reduce UQ.[9] By contrast, the succinate-UQ_1 reductase activity of both SdhB-Ile209 variants is significantly reduced (Table 1). The SdhB-Ile209Ala variant retains 20% of the succinate-UQ_1 reductase activity, but the SdhB-Ile209Lys enzyme retains less than 1% of wild-type activity. The latter result is consistent with *in silico* modeling of the SdhB-Ile209Lys mutation that suggests that the Lys substitution structurally interferes with UQ binding at the quinone-catalytic site (Figure 3). Table 1 also shows that the K_m for UQ_1 in the SdhB-His207Thr and SdhB-Ile209Ala variant enzymes is similar to that of wild-type SQR (unfortunately, the K_m for the SdhB-Ile209Lys variant could not be determined because of the minimal residual activity). Mutation of SdhB-Pro160 to Ala has a lesser effect on UQ reduction than either SdhB-Ile209 variant (Table 1). In addition, a double mutant of SdhB-Pro160Ala and Ile209Ala is approximately 90% compromised in its ability to reduce UQ. Unfortunately, the purified SdhB-Pro160 variants are not sufficiently stable to analyze by pulse radiolysis and were not further investigated. The SdhB-His207 and SdhB-Ile209 variants (Figure 3A−C) were thus chosen for further pulse radiolysis analysis, as amino acid substitutions of these residues introduced gaps (Figure 3B,C compared to wild-type Figure

3A) that might be expected to alter electron-transfer parameters.

The effect of the mutations on the reduction potential of the [3Fe−4S] cluster were ascertained by potentiometric EPR titration of the variants using membranes highly enriched in the expressed proteins. Previous work has shown that mutation of SdhB-His207 to Thr decreases the reduction potential of the [3Fe−4S] cluster by more than 60 to +2 mV, consistent with the loss of the positive charge near the cluster (Table 1).[9,10] These titrations revealed that there was a ∼50 mV increase in the reduction potential of the [3Fe−4S] cluster in the SdhB-Ile209Ala variant (E_m = +120 mV) and a larger increase to E_m = +150 mV in the SdhB-Ile209Lys variant (Table 1). The increase in the latter case can be rationalized by the introduction of a positive charge near the environment of the [3Fe−4S] cluster, as seen in other complex II enzymes.[9,33] The basis for the observed increase in the [3Fe−4S] potential in the SdhB-Ile209Ala variant is less clear, although it may reflect changes in the degree of solvent exposure of the cluster. Regardless, these data show that the reduction potential of the [3Fe−4S] cluster varies over a range of ∼150 mV in the enzyme forms studied in the present work.

Electron Transfer in the SdhB-His207Thr Variant of SQR. The X-ray crystal structure of the SdhB-H207T variant (PDB code 2WP9) has been determined in the presence of the quinone-binding site inhibitor carboxin.[9] In wild-type SQR, the Nδ atom of SdhB-His207 forms a hydrogen bond with one of the heme propionates. Substitution of SdhB-His207 with threonine disrupts this interaction, causing the heme propionate to adopt a different conformation that results in a 1.0 Å larger gap between the [3Fe−4S] cluster and heme. There also appears to be a small increase (∼0.4 Å) in the gap between the proposed UQ-binding site and Thr207 compared to the wild-type histidine. Pulse radiolysis experiments with the SdhB-His207Thr variant reconstituted with UQ reveal only a single intramolecular electron transfer, resulting in the partial reduction of the heme, which contrasts with the two prominent electron-transfer processes seen with wild-type SQR under similar conditions. The initially formed MeN• radical, measured 2 μs after the electron pulse, decays rapidly to a spectrum consistent with Fe/S reduction (minor bleaching in the 400−420 nm region) and some heme reduction (420−440 nm) by 50 μs followed by large spectral changes in this spectral region over 20 ms that we interpret are consistent with intramolecular electron transfer from the [3Fe−4S] cluster to the heme with a rate constant of 160 s^{-1} at 25 °C (Figure 4). This suggests that initial reduction by the MeN• radical is deposited on a redox center that has the ability to reduce the heme, which we suggest is most likely the [3Fe−4S] center. The observed rate constant is some 5-fold slower than the slowest phase seen with the wild-type enzyme (∼840 s^{-1}) and also attributed to equilibration between the [3Fe−4S] cluster and heme.[23] We have also examined the effect of atpenin A5 (AA5), a potent redox-inert inhibitor of SQR[26] that binds at the UQ catalytic site.[34] In the presence of an equimolar concentration of AA5, the rate of electron transfer to the heme in the SdhB-H207T variant is unaffected. Similar results have been obtained using pentachlorophenol, which also binds at the UQ site of the protein.[23,32] These data suggest that electron transfer between the [3Fe−4S] center and heme still occurs in the SdhB-His207Thr variant (albeit at a somewhat reduced rate) but that electron transfer between [3Fe−4S] and UQ has been significantly compromised (as evidenced by the lack of any kinetic phase attributable to it). These data do not eliminate the possibility that this latter process still occurs in this variant, although this would require that k_2 be much smaller than k_3. Overall, these data indicate that SdhB-His207 and bound ubiquinone both facilitate efficient electron transfer to the heme in SQR.

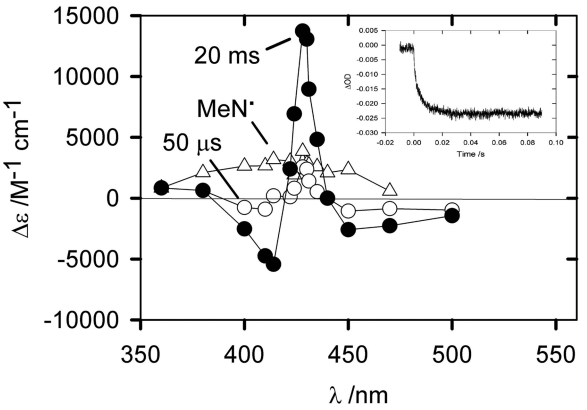

Figure 4. Time-resolved spectral changes following formation of the MeN• radical species 2 μs after the pulse radiolysis (3 Gy in 200 ns) of a N_2O-saturated aqueous solution containing SdhB-His207Thr (30 μM), NMN (2.5 mM), formate ions (0.1 M), and phosphate buffer (5 mM, pH 7). Inset: Observations made at 428 nm associated with k_3 ([3Fe−4S] to *b* heme). The absorption spectra are the difference spectra between the radical intermediates and the prereduced protein, whereas the kinetic transients are the observed changes in transmittance with time.

Electron Transfer in SdhB-Ile209 Variants of SQR. The HARLEM analysis indicates that SdhB-Ile209 is central to the electron-transfer pathway from the [3Fe−4S] cluster to UQ. Two amino acid substitutions were therefore constructed to examine their effect on electron-transfer kinetics: an SdhB-Ile209Ala variant that *in silico* analysis suggested should increase the through-space gap from Ile209 to UQ by 2 Å (from 3.1 to 5.1 Å) and an SdhB-Ile209Lys variant in which *in silico* analysis suggests that the lysine residue partially occludes the quinone-binding site (and also introduces a positive charge at the site).

Pulse radiolysis experiments with the SdhB-Ile209Ala variant revealed only a single intramolecular electron transfer, similar to that seen with the SdhB-His207Thr variant, although with the SdhB-Ile209Ala variant, the observed rate constant is smaller, ∼80 s^{-1} (Figure 5). This rate constant was unchanged when UQ was replaced with AA5, indicating that electron transfer between the [3Fe−4S] and heme is again being observed. With UQ bound, the SdhB-Ile209Lys variant exhibited two kinetic phases, one with a rate constant of 252 ± 44 s^{-1} and the other with a slower rate constant of 47 ± 5 s^{-1} (Figure 6). In the absence of UQ (i.e., with an empty UQ-binding site), a single rate constant of 249 ± 13 s^{-1} was observed, similar to the faster phase observed in wild-type enzyme in the presence of quinone. Lastly, addition of a stoichiometric amount of AA5 to the SdhB-Ile209Lys variant also yielded only a single kinetic phase with a rate constant of 234 ± 11 s^{-1}. These data indicate that the faster of the processes observed with the SdhB-Ile209Lys involves electron transfer between the [3Fe−4S] cluster and heme, with the much slower rate (∼47 s^{-1}) seen with UQ being assigned to electron transfer between the [3Fe−4S] cluster and the quinone. This may suggest that the quinone-binding site in the SdhB-Ile209Lys variant is partially occupied and that there

dx.doi.org/10.1021/bi401630m | *Biochemistry* 2014, 53, 1637−1646

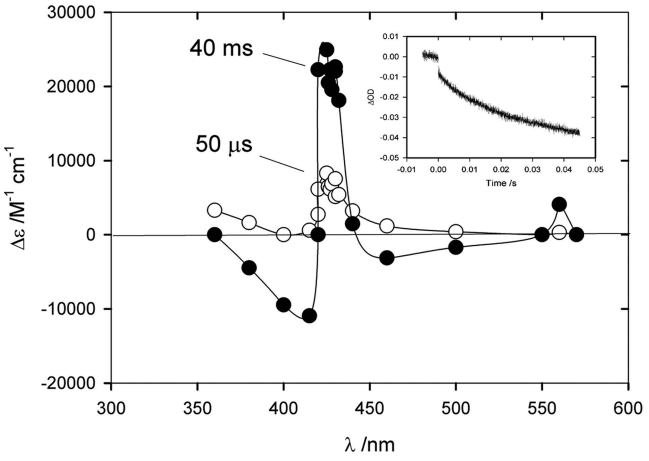

Figure 5. Time-resolved spectral changes following formation of the MeN• radical species, formed as in Figure 4, with SdhB-Ile209Ala (56 μM). Inset: Observations made at 428 nm associated with k_3 ([3Fe−4S] to *b* heme).

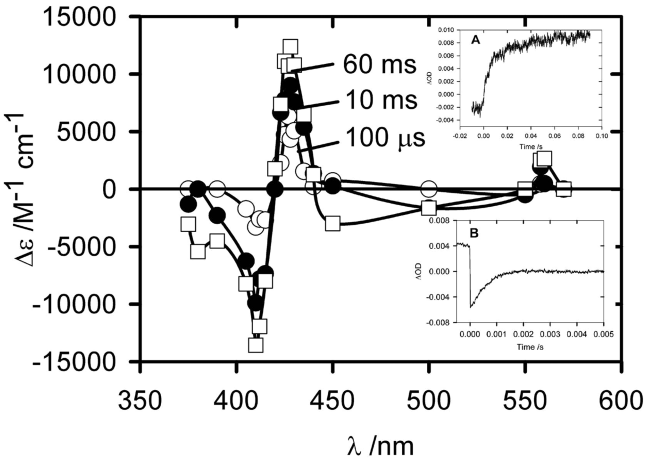

Figure 6. Time-resolved spectral changes following reaction of the MeN• radical species, formed as in Figure 4, with SdhB-Ile209Lys (42 μM). Insets: Observations made at 405 nm; (A) biphasic transient exhibiting slow section associated with k_2 ([3Fe−4S] to UQ) and the residuals from its exponential fit used in generating (B), which is the fast section associated with k_3 ([3Fe−4S] to *b* heme).

is a slow equilibration between the [3Fe−4S] and UQ even with the electron-transfer pathway perturbed by the mutation.

Thermodynamic and Marcus Parameters for Electron Transfer. Assuming that the observed intramolecular rate constants reflect an approach to equilibrium between specific pairs of redox-active centers, individual rate constants for forward and reverse reactions between each redox-active center can be calculated using the known reduction potentials for the centers (see Supporting Information Table S1). Thermodynamic parameters governing all three kinetic pathways in the wild-type enzyme, A, E_{act}, $\Delta G^{\ddagger}$, and $\Delta S^{\ddagger}$, were obtained from transition-state theory using Arrhenius and Eyring plots of the dependence of electron transfer on temperature. Data for electron transfer between the [3Fe−4S] cluster and heme for the SdhB-His207Thr and -Ile209Ala variants as well as electron transfer between the [3Fe−4S] cluster and UQ in the case of the SdhB-Ile209Lys variant were similarly analyzed (Table 2). The Eyring pre-exponential term, A (s^{-1}), contains the dimensionless transmission coefficient, κ, which represents the fraction of molecules achieving the transition state that subsequently proceed to products. The activation energy, E_{act}, for the slowed [3Fe−4S] to UQ phase in the SdhB-Ile209Lys variant is raised considerably relative to wild-type enzyme. The free energy change, $\Delta G^{\ddagger}$, for all phases is similar, whereas the large negative changes in entropy, $\Delta S^{\ddagger}$, most likely arises from charge separation (transfer from the initially reduced [3Fe−4S] cluster) and charge delocalization at equilibrium.

An analysis of diabatic electron transfer in SQR using Marcus theory (eqs 1 and 2) yields information on the effect of site-directed mutagenesis on the reorganization energy, λ, electronic coupling, H_{ab}, and the attenuation coefficient, β.[35]

$$k = \frac{4\pi^2}{h}\frac{{H_{ab}}^2}{\sqrt{(4\pi\lambda k_B T)}}\exp -\frac{(\lambda - \Delta E_0)^2}{(4\lambda k_B T)} \quad (1)$$

Because the driving force of electron transfer for each of the three intramolecular electron transfer processes being examined is small, varying between 0.05 and 0.11 eV, it is valid to plot $\ln(kT^{1/2})$ versus $1/T$ to obtain the Marcus pre-exponential factor, A_M, from the intercept and the activation energy, E_M, from the slope of the plot ($m = -E_M/k_B$). Plots for the [3Fe−4S]/UQ and [3Fe−4S]/heme electron-transfer events in wild-type enzyme are presented in Figure 7, and the derived data for the wild-type and mutant enzymes are given in Table 3. Because $\Delta E_0 \ll \lambda$, then $\lambda \approx 4\Delta E_0$, and H_{ab} can be calculated. It has been proposed[35−37] that the maximum for $k = 1.0 \times 10^{13}$ s^{-1} when λ is independent of distance, D. Using the rate constants observed at 25 °C and the distances between the redox-active centers established by the X-ray crystal structure,[5] it is possible to calculate the attenuation coefficient, β, from eq 2 (Table 3).

$$k = 1.0 \times 10^{13}\exp(-\beta D)\exp(-E_M/k_B T) \quad (2)$$

The pre-exponential factors derived from Arrhenius and Marcus-type plots are related, A (s^{-1}) and A_M ($K^{1/2}$ s^{-1}), with A being slightly smaller because of the effect of κ. As for the E_{act} data, the E_M values for [3Fe−4S]/heme electron transfer are similar for wild-type and variants, whereas E_M for [3Fe−4S]/UQ electron transfer with the SdhB-Ile209Lys variant is raised

Table 2. Thermodynamic Parameters Obtained from Arrhenius and Eyring Plots

protein	kinetic pathway	A (s^{-1})	E_{act} (eV)	$\Delta G^{\ddagger}$ (eV)	$\Delta S^{\ddagger}$ (eV K^{-1})
wild-type	1	$1.29 \pm 0.05 \times 10^9$	0.284 ± 0.021	0.497 ± 0.057	$-8.15 \pm 0.07 \times 10^{-4}$
	2	$3.35 \pm 0.20 \times 10^8$	0.278 ± 0.031	0.578 ± 0.121	$-7.12 \pm 1.30 \times 10^{-4}$
	3	$4.37 \pm 0.30 \times 10^9$	0.391 ± 0.039	0.531 ± 0.086	$-9.33 \pm 1.03 \times 10^{-4}$
His207Thr	3	$7.84 \pm 0.87 \times 10^8$	0.383 ± 0.059	0.640 ± 0.176	$-8.62 \pm 1.95 \times 10^{-4}$
Ile209Ala	3	$1.40 \pm 0.04 \times 10^{10}$	0.494 ± 0.016	0.358 ± 0.036	$-5.43 \pm 0.53 \times 10^{-4}$
Ile209Lys	2	$4.97 \pm 0.72 \times 10^{10}$	0.545 ± 0.092	0.673 ± 0.302	$-5.04 \pm 3.09 \times 10^{-4}$
	3	$3.58 \pm 0.22 \times 10^9$	0.422 ± 0.034	0.614 ± 0.079	$-7.30 \pm 1.15 \times 10^{-4}$

dx.doi.org/10.1021/bi401630m | *Biochemistry* 2014, 53, 1637−1646

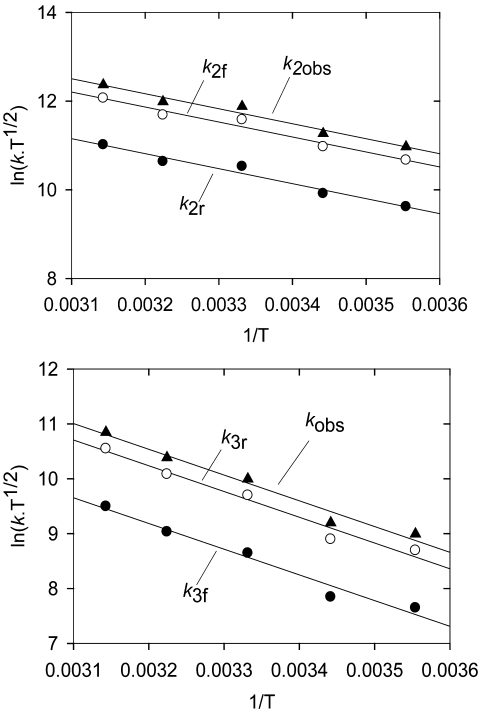

Figure 7. Kinetic plots after Marcus theory of the observed rate constants of intramolecular electron transfer in wild-type SQR as a function of temperature for two kinetic pathways. Upper panel: kinetic pathway 2 ([3Fe−4S]/UQ). Lower panel: kinetic pathway 3 ([3Fe−4S] to *b* heme). Data for k_f and k_r are derived from k_{obs} as a function of the ΔE_0 between the donor and acceptor redox-active centers. Data points are the average of three separate measurements at each temperature.

compared to wild-type enzyme. The derived E_{act} and E_M values are the same within experimental error for all phases studied. Of particular interest are the effect of the amino acid substitutions on λ and β. Whereas these parameters are unchanged for [3Fe−4S]/heme electron transfer in the ShdB-His207Thr and -Ile209Lys variant enzymes compared to wild-type enzyme (thus providing additional support of the assignment of this phase as being due to electron equilibration between the [3Fe−4S] cluster and heme), the slow electron transfer between [3Fe−4S] and UQ in the SdhB-Ile209Lys variant can be attributed to a large increase in λ even though β values are significantly smaller (Table 3). There is also an increase in λ for the [3Fe−4S]/heme phase (kinetic phase 3, Table 3) in the Ile209Ala variant, but in this case, there is a much smaller change in β compared to wild-type enzyme. The determined β values of ∼1.3 $Å^{-1}$ in the UQ/heme (kinetic phase 1, Table 3) and [3Fe−4S]/UQ (kinetic phase 2, Table 3) in the wild-type protein are similar to values found for diabatic electron transfer in many biological systems.[38] There is no correlation between H_{ab} values and k values, although the H_{ab} values (Table 3) are $\ll k_B T$, indicating that the donor and acceptor centers are weakly coupled and that electron transfer occurs via quantum mechanical tunneling.

DISCUSSION

In this study, one-electron reduction of SQR by pulse radiolysis was used to define thermodynamic and other controlling parameters for electron transfer between the [3Fe−4S], UQ, and heme centers of the enzyme, thus providing a full description of these electron-transfer pathways in the enzyme. Previous work using wild-type SQR[23] has shown that the major site of reduction upon reaction of the proximal reductant (the $MeN^{\bullet}$ radical) is at the [3Fe−4S] cluster, with some reduction also occurring at the UQ center. This models the physiological reduction of the [3Fe−4S] center following oxidation of succinate by the fully oxidized enzyme, where electrons are transferred from the reduced FAD moiety individually through the three Fe−S centers of SQR to the high-potential [3Fe−4S] center. Time-resolved spectrophotometry reveals that an electron deposited on the [3Fe−4S] center rapidly equilibrates between it, the UQ, and heme. Because the spatial distribution and reduction potentials of these three centers are known, the system lends itself to a quantitative analysis of the factors controlling intramolecular electron transfer in a multicentered redox-active protein. The data presented in the current study allow us to modify our previous model[23] in which we had suggested that the favored electron-transfer pathway was from the [3Fe−4S]−heme−UQ.[23] This suggestion was influenced by using a high concentration of the weaker-binding inhibitor pentachlorophenol (PCP), which most likely only partially displaced UQ. Using the site-directed variants of SQR and the potent quinone-site inhibitor atpenin A5, the pulse radiolysis and steady-state kinetic data suggest that the preferred electron-transfer pathway is from the [3Fe−4S] to UQ and then to the *b* heme (Figure 1). Support for this conclusion comes from the observation of a larger initial reduction of the heme (as evidenced by the increase in absorbance at 420−430 nm) at the end of the fast reduction of the protein by the $MeN^{\bullet}$ radical when UQ is present compared to when UQ is removed or its site is blocked by atpenin A5 (data not shown). Thus, the occupancy of the UQ site clearly influences the reduction of the heme. The data also show that when the UQ site is perturbed by either mutation or occluded with an inhibitor electron transfer from the [3Fe−4S] to the *b* heme does occur, consistent with our previous model.[23]

In the current study, the program HARLEM was used to identify potential paths for electron transfer between the [3Fe−4S] cluster, UQ, and heme as well as the amino acid residues likely to be important for rapid equilibration of electrons

Table 3. Electron-Transfer Parameters Obtained from Marcus Theory Plots

protein	kinetic pathway	A_M ($K^{1/2}$ s^{-1})	E_M (eV)	λ (eV)	β ($Å^{-1}$)	H_{ab} (eV)
wild-type	1	$3.65 \pm 0.12 \times 10^{10}$	0.296 ± 0.039	1.180 ± 0.084	1.302 ± 0.158	$3.697 \pm 0.283 \times 10^{-4}$
	2	$9.55 \pm 0.49 \times 10^{9}$	0.291 ± 0.031	1.164 ± 0.124	1.259 ± 0.185	$1.885 \pm 0.222 \times 10^{-4}$
	3	$1.25 \pm 0.07 \times 10^{11}$	0.404 ± 0.039	1.616 ± 0.156	0.618 ± 0.090	$7.402 \pm 0.836 \times 10^{-4}$
His207Thr	3	$2.26 \pm 0.21 \times 10^{10}$	0.422 ± 0.059	1.688 ± 0.236	0.805 ± 0.296	$3.182 \pm 0.538 \times 10^{-4}$
Ile209Ala	3	$2.89 \pm 0.07 \times 10^{11}$	0.491 ± 0.015	1.964 ± 0.060	0.833 ± 0.034	$1.182 \pm 0.045 \times 10^{-3}$
Ile209Lys	2	$1.36 \pm 0.17 \times 10^{12}$	0.557 ± 0.091	2.228 ± 0.364	0.358 ± 0.063	$2.646 \pm 0.548 \times 10^{-3}$
	3	$9.82 \pm 0.51 \times 10^{10}$	0.434 ± 0.034	1.736 ± 0.136	0.658 ± 0.041	$6.681 \pm 0.626 \times 10^{-4}$

dx.doi.org/10.1021/bi401630m | *Biochemistry* 2014, 53, 1637−1646

between them. In the pulse radiolysis work described here with several SQR variants, the rates of electron transfer between the redox-active centers are indeed observed to be perturbed relative to wild-type enzyme, consistent with the rates observed when the potent quinone-site inhibitor atpenin A5 is present. Substitution of SdhB-His207 with threonine indicates that this residue plays a pivotal role in electron transfer between [3Fe−4S] and UQ and also between [3Fe−4S] and the heme. In the SdhB-His207Thr variant, the gap between the UQ site and the [3Fe−4S] cluster is not increased to the same extent as that between the heme and the [3Fe−4S] cluster; however, the effect on electron transfer is dramatically different, with that involving the [3Fe−4S] cluster and UQ becoming too slow to be measured. Although the thermodynamic and Marcus parameters controlling electron transfer between the [3Fe−4S] cluster and heme are largely unchanged from that of the wild-type enzyme, the pre-exponential factor (A and A_M) is significantly decreased. This is most likely due to the change in orientation of the heme propionates as well as the increased gap between the [3Fe−4S] cluster and the heme, resulting in a decrease in the rate constant for electron transfer between the [3Fe−4S] cluster and heme in the SdhB-His207Thr variant. The SdhB-Ile209Lys variant also has similar thermodynamic and Marcus parameters to the wild-type enzyme for electron transfer between the [3Fe−4S] cluster and heme, but in this case, the electron-transfer process could be followed, and the change in the rate constant for electron transfer correlated with the changes in Marcus parameters. Of interest is the small β value for electron transfer between the [3Fe−4S] cluster and heme that is observed in the SdhB-Ile209Lys variant. A possible efficient pathway between the [3Fe−4S] and heme center in the wild-type enzyme includes a relatively small gap of 2.6 Å between the histidine imidazole and the heme propionate. The dramatic decrease in β for electron transfer between the [3Fe−4S] cluster and UQ in the SdhB-Ile209Lys variant relative to wild-type enzyme suggests that introduction of the positive charge in the variant may perturb the structure of the quinone-binding pocket and this in turn compromises efficient electron transfer. However, electron transfer between the [3Fe−4S] cluster and heme in the SdhB-Ile209Ala variant is only slightly perturbed, consistent with a more modest structural perturbation as compared with the SdhB-Ile209Lys variant.

During the physiological reduction of SQR by succinate, two electrons are introduced to the flavin at the active site, and these are then distributed among the several redox-active centers of the enzyme. Critical to enzyme turnover is the two-electron reduction of UQ to its hydroquinone form, UQH_2, which then departs from the UQ-binding site. Despite the fact that electron transfer between the [3Fe−4S] cluster and UQ is severely compromised in the SdhB- His207Thr variant, it is observed to exhibit near wild-type activity in steady-state succinate:ubiquinone assays (Table 1). In this variant, the reduction potential of the [3Fe−4S] center (+2 mV)[9] is decreased by the mutation to a lower value than that of the heme (+36 mV). Combined with our findings that the [3Fe−4S]/heme electron-transfer parameters are unchanged compared to the wild-type enzyme, this indicates that reduction of UQ can most likely proceed efficiently via the heme. The reduction potential of the [3Fe−4S] cluster in the SdhB-Ile209Lys (+150 mV) and SdhB-Ile209Ala (+125 mV) variants are both considerably higher than those of UQ (+90 mV) and the heme (+36 mV), indicating that efficient reduction of UQ via the heme is unlikely when electron transfer between the [3Fe−4S] cluster and heme is compromised. This is apparent in the decreased activity of both of these variants compared to the wild-type enzyme (Table 1), although structural changes to the UQ-binding site in the SdhB-Ile209Lys variant may also be involved. This analysis also shows that in SQR occupancy of the UQ-binding site is a prerequisite for efficient electron transfer to the heme and that the process involves pure electron tunneling. These latter results are consistent with previous steady-state kinetic studies also suggesting that occupancy of the quinone site is essential for rapid reduction of the heme,[16] but they also suggest that in the wild-type enzyme the electron can rapidly shuttle between the reduced heme and quinone (k_1, Figure 1).

As noted above, during the two-electron oxidation of succinate resulting in formation of $FADH_2$, the electrons sequentially enter the chain of iron−sulfur clusters of SQR. The first electron initially ends up at the highest potential iron sulfur cluster ([3Fe−4S]), and consistent with the data reported here and our previous studies,[16] this is followed by quinone reduction to the stabilized semiquinone, which is in rapid equilibration with the heme. The present work demonstrates that perturbation of the quinone-binding pocket by mutation can significantly influence the rate of heme reduction in complex II. Relevant to this are the data shown in Table 1 for the steady-state kinetics of the SdhB-Pro160 variants that indicates that this residue is also important in electron transfer between the [3Fe−4S] and quinone (consistent with the HARLEM pathway analysis). It should be noted that in humans mutation of the residue equivalent to *E. coli* SdhB-Pro160 (human SdhB-Pro197) has been associated with paraganglio-mas and phaeochromocytoma tumors.[39−41] It has also been noted that of the germline mutations identified in human complex II, those in the SDHB gene are most frequently associated with malignancy and a poor clinical prognosis.[41−43] Recent studies of mammalian complex II have called increasing attention to the role of the enzyme as a generator of reactive oxygen species (ROS).[20,21] Available evidence suggests that both the flavin semiquinone[20,44,45] and ubisemiquinone radical[46−48] are likely sources of ROS. The data presented here show that the rate of electron transfer in complex II is altered by mutations that perturb the quinone-binding region even when they do not significantly affect overall enzyme activity. Because many of the missense substitutions of complex II associated with human diseases map to the quinone-binding region of the enzyme,[22,49] it seems likely that alteration of electron distribution in the quinone-binding domain, although having only subtle effects on activity, may nevertheless increase the propensity for the enzyme to produce ROS.

In summary, these studies show that complex II conserved amino acids SdhB-His207, SdhB-Ile209, and SdhB-Pro160 of the *E. coli* enzyme are part of the preferred electron-transfer pathway.

■ ASSOCIATED CONTENT

Supporting Information

Kinetic data and electron-transfer parameters obtained from Marcus theory plots. This material is available free of charge via the Internet at http://pubs.acs.org.

■ AUTHOR INFORMATION

Corresponding Authors

*(R.F.A.) Tel: +64-9-923-8315; E-mail: r.anderson@auckland.ac.nz.

*(G.C.) Tel: 415-221-4810 ext. 4416; Fax: (415) 750-6959; E-mail: gary.cecchini@ucsf.edu.

Funding

The work in the authors' laboratories was supported in whole or in part by the Department of Veterans Affairs Biomedical Laboratory Research and Development Merit Award (BX001077), the National Institutes of Health (GM61606), the U.S. Department of Energy (DE-SC0010666), and the Canadian Institutes of Health Research (MOP89735).

Notes

The authors declare no competing financial interest.

■ ABBREVIATIONS

FAD, flavin adenine dinucleotide; SQR, succinate-quinone oxidoreductase; QFR, quinol-fumarate oxidoreductase; NMN, *N*-methylnicotinamide; $MeN^{\bullet}$, one-electron reduced NMN; UQ, ubiquinone; USQ, ubisemiquinone; UHQ, ubihydoquinone; UQH_2, ubiquinol; Gy, gray; PCP, pentachlorophenol; EDTA, ethylenediaminetetraacetic acid; PES, phenazine ethosulfate; EPR, electron paramagnetic resonance spectroscopy; AA5, atpenin A5

■ REFERENCES

(1) Cecchini, G. (2003) Function and structure of complex II of the respiratory chain. *Annu. Rev. Biochem. 72*, 77−109.

(2) Hagerhall, C. (1997) Succinate:quinone oxidoreductases. Variations on a conserved theme. *Biochim. Biophys. Acta 1320*, 107−141.

(3) Bayley, J. P., van Minderhout, I., Hogendoorn, P. C., Cornelisse, C. J., van der Wal, A., Prins, F. A., Teppema, L., Dahan, A., Devilee, P., and Taschner, P. E. (2009) Sdhd and SDHD/H19 knockout mice do not develop paraganglioma or pheochromocytoma. *PLoS One 4*, e7987-1−e7987-7.

(4) Lancaster, C. R. (2002) Succinate:quinone oxidoreductases: An overview. *Biochim. Biophys. Acta 1553*, 1−6.

(5) Yankovskaya, V., Horsefield, R., Tornroth, S., Luna-Chavez, C., Miyoshi, H., Leger, C., Byrne, B., Cecchini, G., and Iwata, S. (2003) Architecture of succinate dehydrogenase and reactive oxygen species generation. *Science 299*, 700−704.

(6) Sun, F., Huo, X., Zhai, Y., Wang, A., Xu, J., Su, D., Bartlam, M., and Rao, Z. (2005) Crystal structure of mitochondrial respiratory membrane protein complex II. *Cell 121*, 1043−1057.

(7) Huang, L. S., Sun, G., Cobessi, D., Wang, A. C., Shen, J. T., Tung, E. Y., Anderson, V. E., and Berry, E. A. (2006) 3-Nitropropionic acid is a suicide inhibitor of mitochondrial respiration that, upon oxidation by complex II, forms a covalent adduct with a catalytic base arginine in the active site of the enzyme. *J. Biol. Chem. 281*, 5965−5972.

(8) Maklashina, E., and Cecchini, G. (2010) The quinone-binding and catalytic site of complex II. *Biochim. Biophys. Acta 1797*, 1877−1882.

(9) Ruprecht, J., Iwata, S., Rothery, R. A., Weiner, J. H., Maklashina, E., and Cecchini, G. (2011) Perturbation of the quinone-binding site of complex II alters the electronic properties of the proximal [3Fe−4S] iron-sulfur cluster. *J. Biol. Chem. 286*, 12756−12765.

(10) Tran, Q. M., Rothery, R. A., Maklashina, E., Cecchini, G., and Weiner, J. H. (2007) *Escherichia coli* succinate dehydrogenase variant lacking the heme b. *Proc. Natl. Acad. Sci. U.S.A. 104*, 18007−18012.

(11) Oyedotun, K. S., Sit, C. S., and Lemire, B. D. (2007) The *Saccharomyces cerevisiae* succinate dehydrogenase does not require heme for ubiquinone reduction. *Biochim. Biophys. Acta 1767*, 1436−1445.

(12) Maklashina, E., Rothery, R. A., Weiner, J. H., and Cecchini, G. (2001) Retention of heme in axial ligand mutants of succinate-ubiquinone oxidoreductase (complex II) from *Escherichia coli*. *J. Biol. Chem. 276*, 18968−18976.

(13) Kita, K., Vibat, C. R., Meinhardt, S., Guest, J. R., and Gennis, R. B. (1989) One-step purification from *Escherichia coli* of complex II (succinate:ubiquinone oxidoreductase) associated with succinate-reducible cytochrome b556. *J. Biol. Chem. 264*, 2672−2677.

(14) Hatefi, Y., and Galante, Y. M. (1980) Isolation of cytochrome b560 from complex II (succinate·ubiquinone oxidoreductase) and its reconstitution with succinate dehydrogenase. *J. Biol. Chem. 255*, 5530−5537.

(15) Yu, L., Xu, J. X., Haley, P. E., and Yu, C. A. (1987) Properties of bovine heart mitochondrial cytochrome b560. *J. Biol. Chem. 262*, 1137−1143.

(16) Tran, Q. M., Rothery, R. A., Maklashina, E., Cecchini, G., and Weiner, J. H. (2006) The quinone binding site in *Escherichia coli* succinate dehydrogenase is required for electron transfer to the heme b. *J. Biol. Chem. 281*, 32310−32317.

(17) Maklashina, E., Berthold, D. A., and Cecchini, G. (1998) Anaerobic expression of *Escherichia coli* succinate dehydrogenase: Functional replacement of fumarate reductase in the respiratory chain during anaerobic growth. *J. Bacteriol. 180*, 5989−5996.

(18) Horsefield, R., Yankovskaya, V., Tornroth, S., Luna-Chavez, C., Stambouli, E., Barber, J., Byrne, B., Cecchini, G., and Iwata, S. (2003) Using rational screening and electron microscopy to optimize the crystallization of succinate:ubiquinone oxidoreductase from *Escherichia coli*. *Acta Crystallogr., Sect. D: Biol. Crystallogr. 59*, 600−602.

(19) Page, C. C., Moser, C. C., Chen, X., and Dutton, P. L. (1999) Natural engineering principles of electron tunnelling in biological oxidation-reduction. *Nature 402*, 47−52.

(20) Quinlan, C. L., Orr, A. L., Perevoshchikova, I. V., Treberg, J. R., Ackrell, B. A., and Brand, M. D. (2012) Mitochondrial complex II can generate reactive oxygen species at high rates in both the forward and reverse reactions. *J. Biol. Chem. 287*, 27255−27264.

(21) Drose, S. (2013) Differential effects of complex II on mitochondrial ROS production and their relation to cardioprotective pre- and postconditioning. *Biochim. Biophys. Acta 1827*, 578−587.

(22) Iverson, T. M., Maklashina, E., and Cecchini, G. (2012) Structural basis for malfunction in complex II. *J. Biol. Chem. 287*, 35430−35438.

(23) Anderson, R. F., Hille, R., Shinde, S. S., and Cecchini, G. (2005) Electron transfer within complex II. Succinate:ubiquinone oxidoreductase of *Escherichia coli*. *J. Biol. Chem. 280*, 33331−33337.

(24) Hille, R., and Anderson, R. F. (1991) Electron transfer in milk xanthine oxidase as studied by pulse radiolysis. *J. Biol. Chem. 266*, 5608−5615.

(25) Anderson, R. F., Jang, M. H., and Hille, R. (2000) Radiolytic studies of trimethylamine dehydrogenase. Spectral deconvolution of the neutral and anionic flavin semiquinone, and determination of rate constants for electron transfer in the one-electron reduced enzyme. *J. Biol. Chem. 275*, 30781−30786.

(26) Miyadera, H., Shiomi, K., Ui, H., Yamaguchi, Y., Masuma, R., Tomoda, H., Miyoshi, H., Osanai, A., Kita, K., and Omura, S. (2003) Atpenins, potent and specific inhibitors of mitochondrial complex II (succinate-ubiquinone oxidoreductase). *Proc. Natl. Acad. Sci. U.S.A. 100*, 473−477.

(27) Westenberg, D. J., Gunsalus, R. P., Ackrell, B. A., Sices, H., and Cecchini, G. (1993) *Escherichia coli* fumarate reductase frdC and frdD mutants. Identification of amino acid residues involved in catalytic activity with quinones. *J. Biol. Chem. 268*, 815−822.

(28) Anderson, R. F., and Patel, K. B. (1984) Radical cations of some low-potential viologen compounds. *J. Chem. Soc., Faraday Trans. 1 80*, 2693−2702.

(29) Maklashina, E., and Cecchini, G. (1999) Comparison of catalytic activity and inhibitors of quinone reactions of succinate dehydrogenase (succinate-ubiquinone oxidoreductase) and fumarate reductase (menaquinol-fumarate oxidoreductase) from *Escherichia coli*. *Arch. Biochem. Biophys. 369*, 223−232.

(30) Rothery, R. A., and Weiner, J. H. (1996) Interaction of an engineered [3Fe−4S] cluster with a menaquinol binding site of *Escherichia coli* DMSO reductase. *Biochemistry 35*, 3247−3257.

(31) Maklashina, E., Iverson, T. M., Sher, Y., Kotlyar, V., Andrell, J., Mirza, O., Hudson, J. M., Armstrong, F. A., Rothery, R. A., Weiner, J. H., and Cecchini, G. (2006) Fumarate reductase and succinate oxidase activity of *Escherichia coli* complex II homologs are perturbed differently by mutation of the flavin binding domain. *J. Biol. Chem. 281*, 11357−11365.
(32) Ruprecht, J., Yankovskaya, V., Maklashina, E., Iwata, S., and Cecchini, G. (2009) Structure of *Escherichia coli* succinate:quinone oxidoreductase with an occupied and empty quinone-binding site. *J. Biol. Chem. 284*, 29836−29846.
(33) Cheng, V. W., Ma, E., Zhao, Z., Rothery, R. A., and Weiner, J. H. (2006) The iron-sulfur clusters in *Escherichia coli* succinate dehydrogenase direct electron flow. *J. Biol. Chem. 281*, 27662−27668.
(34) Horsefield, R., Yankovskaya, V., Sexton, G., Whittingham, W., Shiomi, K., Omura, S., Byrne, B., Cecchini, G., and Iwata, S. (2006) Structural and computational analysis of the quinone-binding site of complex II (succinate-ubiquinone oxidoreductase): A mechanism of electron transfer and proton conduction during ubiquinone reduction. *J. Biol. Chem. 281*, 7309−7316.
(35) Marcus, R. A., and Sutin, N. (1985) Electron transfers in chemistry and biology. *Biochim. Biophys. Acta 811*, 265−322.
(36) Closs, G. L., and Miller, J. R. (1988) Intramolecular long-distance electron transfer in organic molecules. *Science 240*, 440−447.
(37) Moser, C. C., Keske, J. M., Warncke, K., Farid, R. S., and Dutton, P. L. (1992) Nature of biological electron transfer. *Nature 355*, 796−802.
(38) Davidson, V. L. (2000) What controls the rates of interprotein electron-transfer reactions. *Acc. Chem. Res. 33*, 87−93.
(39) Bayley, J. P., Devilee, P., and Taschner, P. E. (2005) The SDH mutation database: an online resource for succinate dehydrogenase sequence variants involved in pheochromocytoma, paraganglioma and mitochondrial complex II deficiency. *BMC Med. Genet. 6*, 39-1−39-6.
(40) Lima, J., Feijao, T., Ferreira da Silva, A., Pereira-Castro, I., Fernandez-Ballester, G., Maximo, V., Herrero, A., Serrano, L., Sobrinho-Simoes, M., and Garcia-Rostan, G. (2007) High frequency of germline succinate dehydrogenase mutations in sporadic cervical paragangliomas in northern Spain: Mitochondrial succinate dehydrogenase structure-function relationships and clinical-pathological correlations. *J. Clin. Endocrinol. Metab. 92*, 4853−4864.
(41) Burnichon, N., Rohmer, V., Amar, L., Herman, P., Leboulleux, S., Darrouzet, V., Niccoli, P., Gaillard, D., Chabrier, G., Chabolle, F., Coupier, I., Thieblot, P., Lecomte, P., Bertherat, J., Wion-Barbot, N., Murat, A., Venisse, A., Plouin, P. F., Jeunemaitre, X., and Gimenez-Roqueplo, A. P. (2009) The succinate dehydrogenase genetic testing in a large prospective series of patients with paragangliomas. *J. Clin. Endocrinol. Metab. 94*, 2817−2827.
(42) Amar, L., Baudin, E., Burnichon, N., Peyrard, S., Silvera, S., Bertherat, J., Bertagna, X., Schlumberger, M., Jeunemaitre, X., Gimenez-Roqueplo, A. P., and Plouin, P. F. (2007) Succinate dehydrogenase B gene mutations predict survival in patients with malignant pheochromocytomas or paragangliomas. *J. Clin. Endocrinol. Metab. 92*, 3822−3828.
(43) Timmers, H. J., Kozupa, A., Eisenhofer, G., Raygada, M., Adams, K. T., Solis, D., Lenders, J. W., and Pacak, K. (2007) Clinical presentations, biochemical phenotypes, and genotype-phenotype correlations in patients with succinate dehydrogenase subunit B-associated pheochromocytomas and paragangliomas. *J. Clin. Endocrinol. Metab. 92*, 779−786.
(44) Imlay, J. A. (1995) A metabolic enzyme that rapidly produces superoxide, fumarate reductase of *Escherichia coli*. *J. Biol. Chem. 270*, 19767−19777.
(45) Messner, K. R., and Imlay, J. A. (2002) Mechanism of superoxide and hydrogen peroxide formation by fumarate reductase, succinate dehydrogenase, and aspartate oxidase. *J. Biol. Chem. 277*, 42563−42571.
(46) Guo, J., and Lemire, B. D. (2003) The ubiquinone-binding site of the *Saccharomyces cerevisiae* succinate-ubiquinone oxidoreductase is a source of superoxide. *J. Biol. Chem. 278*, 47629−47635.
(47) Szeto, S. S., Reinke, S. N., Sykes, B. D., and Lemire, B. D. (2007) Ubiquinone-binding site mutations in the *Saccharomyces cerevisiae* succinate dehydrogenase generate superoxide and lead to the accumulation of succinate. *J. Biol. Chem. 282*, 27518−27526.
(48) Paranagama, M. P., Sakamoto, K., Amino, H., Awano, M., Miyoshi, H., and Kita, K. (2010) Contribution of the FAD and quinone binding sites to the production of reactive oxygen species from *Ascaris suum* mitochondrial complex II. *Mitochondrion 10*, 158−165.
(49) Hoekstra, A. S., and Bayley, J. P. (2013) The role of complex II in disease. *Biochim. Biophys. Acta 1827*, 543−551.